Medical Image Segmentation Based Image Compression with Secure Cloud Data Storage

P. Renukadevi1 , M. Syed Mohamed2

1Research Scholar, Reg.No 19111252302005, Department of Information Technology, Sri Ram Nallamani Yadava College of Arts and Science(Affiliated toManonmaniam Sundaranar University Tirunelveli) Tenkasi Tamil Nadu, India 2Assistant Professor, Department of Information Technology, Sri Ram Nallamani Yadava College of Arts and Science (Affiliated to Manonmaniam Sundaranar University Tirunelveli) Tenkasi Tamil Nadu, India

Article Info
Page Number: 1074 – 1095
Publication Issue:
Vol. 71 No. 3 (2022)

Abstract:-

Scanning rates and distinction rates in imaging equipment have been considerably improved with the development of CT, MRI, EBCT, SMRI, etc. Medical images may be extensively processed using compression techniques to the benefit of the image information and to improve the diagnosis, by means of de noises, enhancements, edge extraction, etc . Since medical images are available in digital format, the technology is to produce more time-saving and cost-effective image compression to minimise the volume of image data. This article aims at proposing a novel approach for compression of the images, which is processed in different sequences. Here Preprocessing is performed by contrast Curvature based shearlet filter with Contrast Limited Golay Histogram Equalization is used. After the pre-processing process is the image segmentation and is handled by Adaptive Contour in depth watershed segmentation Model (ACIWS), which divides or segments the image into two regions: ROI (Region of Interest) and non ROI. In this, the wavelet iterative cuckoo herd optimization algorithm for compressing the ROI and Non ROI regions . Then the image can be securely stored in a cloud by using crack tetrolet elgamal algorithm. Subsequently, the compressed image is subjected for image decompression, which will be the reverse process of compression. Finally, the original image is attained precisely. The whole experimentation can carried out in a 3DIRCADB public available liver cancer dataset. The simulations were run in the MATLAB simulation environment and included metrics for both the proposed and current protocols. It is obvious from the comparison that the present mechanism performs poorly when compared to the suggested method.

Article History
Article Received: *12 January 2022*
Revised: *25 February 2022*
Accepted: *20 April 2022*
Publication: *09 June 2022*

Keywords:- Image Compression, contrast Curvature based shearlet filter , Contrast Limited Golay Histogram Equalization, Adaptive Contour in depth watershed segmentation, wavelet iterative cuckoo herd optimization algorithm, crack tetrolet elgamal algorithm

1.INTRODUCTION

The simple, quick and reliable digital transmission and storage of health and biological images would be a key advantage for the medical professions. The second opinion might be easily available to patients in remote regions. Patients readmitted to hospitals might get immediate access to prior imaging results. Installments around the hospital can simultaneously access imagery studies on displays rather than waiting for others to complete using hardcopy images. Long-term digital preservation or fast transmission is expensive without the use of compression to decrease the file size. A 4096 to 4096 pixel x 16 bpp can be used, say, to digitize an analogue mammograms. For instance. It's a 33 megabyte (MB). The original image may be correctly recovered using a lossless compression from the compressed format; this does not have the loss coding, but a lot greater compression. Nevertheless, many members of the medical and scientific community suspect loss systems; alterations in pictures might lead to loss of diagnosis or value of the study. Many doctors believe they have little confidence in loss-compression, which is largely excellent, however can include inacceptable medical devices in the image without notification. Following the segmentation of an image in distinct locations, a compression approach might give various levels of reconstruction quality (whether automatically or manually). The essential features for medical or scientific diagnosis can be kept properly (losslessly) despite attaining a high overall compression in lowest-level regions. The key for physicians and scientists to entrust images to compression may be this coding that we call regionally loss-free or loss-free ROI coding. In radiology, image compression is typically discussed in three different uses: primary diagnostic compression (for quick transmission), primary diagnostic compression (for long-term storage) and data base browsing compressive analysis (where progressivity would be useful). The most challenging use of loss compression is compression before initial diagnosis. It could, however, be beneficial if the processor is at a distant site and compression without loss cannot be employed. For example, the circumstances of the patient might necessitate such quick actions that it is impossible to counteract the time required to transmit original images without loss or to ensure bandwidth is not sufficient for reliable lossless video transmission. Compression may be helpful in the long term digital preservation following first diagnosis. Because a picture may be used for primary interpretation to separate the region, it's easy to understand how regionally based coding could be useful. A third application of compression is to send photos over a network in stages. With each extra bit, progressive coding improves picture quality. Early image versions can demonstrate that the image is boring, and the transmission can then be 'buddled.' Progressive coding can be made lossless in the future, so the picture will look exactly like the original if the user waits long enough (e.g. 30s), but in the short time, the picture (e.g. 0.5 s) will sufficient. Many methods for lossless picture pixel bit compression have been presented in the past, however the image quality was not as good as it was in the original image. Hence here in this paper we present a lossless compression approach along with segmentation based on the safe compression of the image based on wavelet iterative cuckoo herd optimization, Adaptive Contour in depth watershed segmentation and crack tetrolet elgamal algorithm. The rest of the paper can be organized as follows, section 1 depicts the basic introduction about the segmentation with lossless image compression and the secure cloud storage process. The related existing methodologies were depicted in section 2. The problem definition was depicted in section 3. The technique used for the ROI segmentation with secure lossless image compression is defined in Section 4, while the findings and explanation for the study are in Section 5. Section 6 ultimately summarizes the paper.

2.RELATED WORKS

[1] Present RDonet, an unique technique for achieving similar compression results using full-image autoencoders, through multiple levels of hierarchy which are adaptively transmitted following optimisation of external rates. **[2]** Proposing slimming auto-encoders (SlimCAEs), which are combined in terms of rate (R) and distortion (D). Once trained, encoders and decoders can be performed at various speeds and complexity. We demonstrate that successful deployment of SlimCAEs needs appropriate capacity-specific RD compromise. [3] Review the various ways of wavelet modification used for medical pictures. [4] Image encryption should be fine-tuned and compressed. The main goal of the ASFSCSLEC-DNL technique was to improve the degree of safety in medical picture transmission. In deep feed-forwards artificial neural networks, the ASFSCSLEC-DNL technology was utilised for pre-processing, encryption, and multi-layered compression of medical imaging. To criticise the medical image, the adaptive sigma filter was employed. Synorr certificateless signing was used for the medical picture encryption and signing generation. Finally, the entropy encoding of Levenshtein was used to compress pictures. The compressed picture was then forwarded to the receiver to decompress and decode using the entropy decoding system and certified certificateless decoding Levenshtein. **[5]** The prediction approach is done utilizing two identical neural feed-forward networks throughout the compression and decompression stages (FF-NNs). Gravitational search and particle swarm algorithms are both trained using FF-NNs. Lossless (LLP) and near-lossless (NLLP) performance predictions are made for both FF-NN training techniques. The predicted sequence error, or the difference between the actual and anticipated pixel values, is further compressed using a Markov model based arithmetic coding. The recommended technique is tested using the CLEF med 2009 database. **[6]** The medical image is originally split into two sections: ROI and non-ROI areas, with compression techniques given for both. The ROI portions are compressed using a lossless BPG compression technique, while the non-ROI parts are compressed using a lossless BPG. Finally, the reconstructed pictures are created by merging a full compressed image. **[7]** Resent a new method by creating issues with convex smoothing. This is done by splitting the picture into sub-problems. This method. Accordingly, we split a compressed sensing technique to the input picture into sub-problems. This problem is submitted to the problem solver procedure to decrease time, computer complexity, and reconstruction errors after reaching the compressed-sensed image's output. **[8]** Proposes an efficient embedded image coder designed for lossless ROI code at a very high compression ratio based reversibly discrete cosine transform (RDCT). The suggested rearranged structure is nicely combined with a lost zero tree wavelet code (LEZW), motivated by the structure of the wavelet of DCT, whilst the background is greatly compressed utilizing hierarchical (SPIHT) partitioning approach. The coding results demonstrate that the performance of the novel encoder is significantly higher than that of several state of the art still picture compression techniques. **[9]** To achieve adaptive irregular medical image segmentation, the author proposes a hybrid approach that combines geometric and quad trine partitioning. For each region, the least square (LS) predictors are modified (regular subblock or irregular subregion). The proposed adaptive approach takes into account not just spatial correlation between pixels, but also local structural similarity, resulting in efficient compression. **[10]** present a generative architecture for segmentation consisting of a compression network and a segmentation network. **[11]** New methods are given that combine image reduction and enlargement technologies, digital watermarking, and lossless compression standards such as JPEG-LS (JLS) and TIFF formats. [12] The new loss compression technique enhances contourlet compression performance and offers great image quality even at lower bit rates. Standardization and prediction of broken sub band coefficients, in addition to SVD, improve compression efficiency.

3.PROBLEM STATEMENT

An effective and effective algorithm for removing various redundancies from particular types of data is a compression problem from the algorithm point of view. At this point we require a clear understanding of the problem and a new method to address all the existing research gaps with imperishable picture compression.

4.PROPOSED METHODOLOGY

Liver cancer is one of the most frequent kinds of cancer with growing morbidity worldwide. In order for early diagnosis and treatment to increase survival rates, the tools of medical imaging are of significant assistance. Among many various imaging modes, CT is commonly used to diagnose hepatic illness as it can give precise anatomical information to relatively high resolution images. The division of liver and tumors from CT images is an important precondition for early diagnosis, planning and monitoring of hepatic cancer. This studies will thus use the suggested approach to partition the ROI and compress it with safe cloud storage for efficient liver cancer compression without loss.

Dataset

The suggested procedure was tested by means of the public CT dataset, which includes 15 CT volume imaging's of 120 different-size hepatic tumors (3Dircadb (http://www.ircad.fr/research /3dircadb)). With in-plane resolution of 512 x 512 pixels in each sample, pixel spacing, slice thickness, and number of slices ranged from 0.56 to 0.87 mm, 1 to 4 mm, and 74 to 260, respectively, with in-plane resolution of 512 × 512 pixels in each case. Manually segmented tumors were also provided and considered the basic reality. The schematic representation of the suggested methodology was depicted in figure 1.

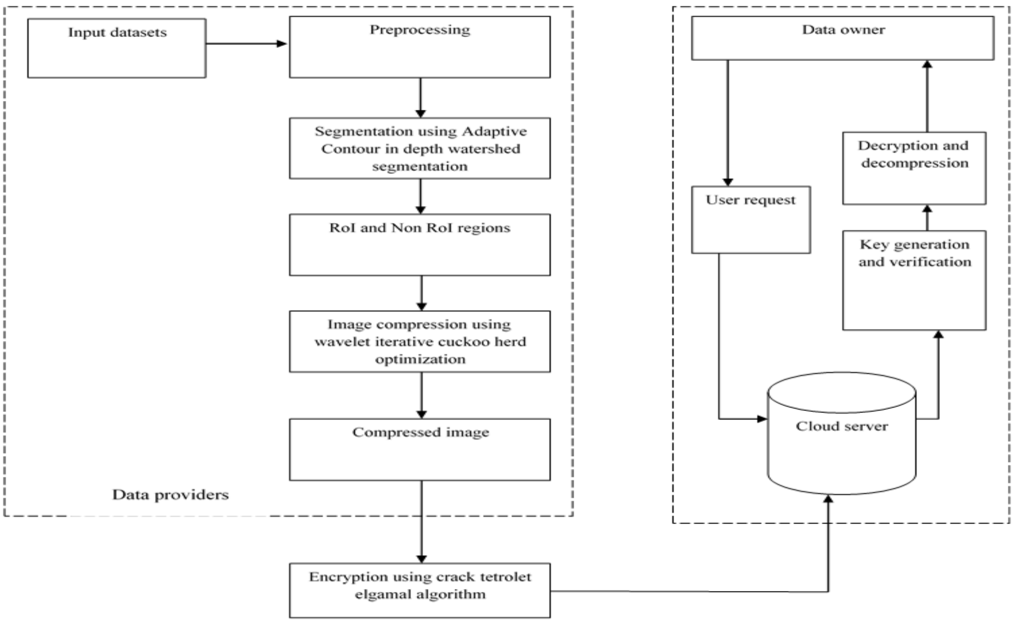

Figure 1 Schematic representation of the suggested methodology

a. Preprocessing

The image processing should be used as an early stage in an advanced technique. It carries out the error treatment, which helps to estimate pixels in the image but may also shape the Curvature by the impulse noise. With the help of all pixels in a picture, it isolates pixels as noise and its neighboring pixels. It is most adaptable to the neighboring pixel size.

This technique will replace the median pixel value of the pixels in the neighborhood passed by a noise labeling test. The Contrast curvature-based shearlet filter is designed to eliminate impulse noise, smooth out other noises and minimize distortion. The filter's performance is shown in the following steps.

Steps

Level Y: $Y1 = GL_{CBS} - GL_{min}$

$Y2 = GL_{CBS} - GL_{max}$

If $Y1 > 0$ and $Y2 < 0$, go to the level B

Else window size should gets increased

If size of the window < $Size_{max}$, repeat level Y

Else output GL_{pq}

Level Z: $Z1 = GL_{pq} - GL_{min}$

$Z2 = GL_{pq} - GL_{max}$

If $Z1 > 0$ AND $Z2 < 0$, output GL_{pq}

Else output GL_{CBS}

Size – Curvature based shearlet filter during operations t helps adjust the size of the area.

G_{armin} – maximum value of gray level in $Size_{pq}$

$_{Lomax}$ – maximum value of gray level in $Size_{pq}$

GL_{med} - median gray levels in $Size_{pq}$

GLP – the gray level at coordinates (p, q)

$Size_{max}$ – the maximum allowed size of $Size_{pq}$

Here which initially in the level X suggested filter can remove the noise, then after noise removal, the Curvature of the image can get shape out fully in level Y. Since the special curvatures are imposed, our filters are 100 or 10000 times faster than traditional solvers in terms of minimizing curvatures. After that histogram of the image can be equalized by using the Contrast iterative Golay Histogram Equalization. Typically, histogram equalization is achieved to increase image consistency. Histogram Equalization is a computerized process used to enhance the contrast of pictures.

The image intensity can be adjusted to enhance the contrast of the image.

D_N = [(Amount of the pixel of intensity n/total number of the pixels)*filter areas]^2 (1)

Where D is the normalized histogram

b. Segmentation

For the Segmentation, the Adaptive Contour in depth watershed segmentation method can be used. The water shed fundamental concept is to depict the hyper-surface curves and surfaces as a zero level range. It provides more precise numerical and fast topological tests: the surface-smoothing method $\emptyset(R, K, D)$ refers to the set-null-level method $\emptyset(R, K, D) = 0$. The whole surface may be viewed within and outside of the curve when using the curve as the boundary. To initialize this operation, the concept of Signed Distance (SDF) function on the surface is as follows equation (2).

$$\emptyset(R, K, D = 0) = G \qquad (2)$$

Where,

G is the shortest distance between the point on the surface and curve.

The general level set function is defined as follows in equation (3)

$$\emptyset_T + gD|\nabla\emptyset| = 0 \qquad (3)$$

Where,

F is the independent function depends on the information of images.

To improve the segmentation process, the independent internal term and the external independent term shall be considered. The gradient flow that reduces the cumulative power function is this growth.

$$E(\emptyset) = \min (E\,[e^T e]) = \min g\,(E\,|\,(t - \sigma)^T (t - \sigma)|) \qquad (4)$$

Where,

E is the controlling parameter.

σ is the Dirac delta function

g is the edge indicator function defined by

$$g_j = \sigma_j(1 - \sigma_j)(t_j - \sigma_j) \qquad (5)$$

I is an image, and g_j is the Gaussian kernel with standard deviation. To find the “watershed ridge lines” in an image by treating it as a surface, where light pixels are high and dark pixels are low.

$$M = \sum_{x,y} wE(R,K,D) \begin{bmatrix} I_{RK}^2 & I_D I_R \\ I_K I_D & I_D^2 \end{bmatrix} \qquad (6)$$

A segmented watershed uses the topography analogy. By using this method the image features can be easily pre-determined. In this research, the intensity of the gradient uses grayscales for the segmentation process. The image velocity gradient has high pixels and low pixels along the boundaries of the object.

$$W^{\mathrm{Segmentation}} = \sum_{\{i.j\}\in Q_2}^{S} M_2(y_i, y_j).\, g_i.\log_{c_i}\emptyset + \gamma \int \mathrm{RKD_i}\, dx \qquad (7)$$

Where $W^{\mathrm{Segmentation}}$ is the watershed segmentation, V is the velocity gradient, y_i, y_j was the low and high pixel value, m represents the number of pixel blocks in the image, $\log_{c_i}$ represents the spatial size of the image, γ represents the frequency coefficient of an image, c_i represents the distance of the pixels. By using the suggested methodology the region and the non-ROI can gets segmented.

c. Image compression

During the compression step, a wavelet iterative cuckoo herd optimization has been used. It is an algorithm that analyses the compression characteristics. This algorithm is recommended as a population-based algorithm to maximize the compression related parameters. There are WICHO instructions: any cuckoo must select the nest randomly and place an egg on each nest. The subsequent generation should move the lowest egg content to the best nest. The host nest number is set, and the host bird tests the cuckoo egg in accordance with the probability of Pa[0,1]. The host bird will either kill it or abandon the nest when eggs from the cuckoo are detected. WICHO is the primary approach to the problem analysis and data modelling of the compression parameter. The Lévy(α) distribution for this function is determined based on:

Lévy class (α) ≈ v= l^{-} α (8)

The Lévy distribution can be simplified by the following equation:

$$\theta \propto \text{Lévyclass}(\alpha) \approx X * (\frac{d}{|u^1/3|})(x_{best-}x_{i)} \quad (9)$$

where X is the Lévy multiplication coefficient, and d and u are deducted from the normal distribution curves.

The wavelet grouping is interpreted as follows: The first phase should concentrate on the training characteristics of the wavelet samples. The Wavelet has the (Class > 3) classes and assumes the X_a be the set of $T_a$and m_a samples in the dimension of DS. The scatter matrix is derived for each and every class between the class m_{bc} and m_{wi_c} and they are defined as follows in the class dispatch matrix,

$m_{wi\_c} = \sum_{a=1}^{CLASS} m_a$; $X_a = \frac{1}{p_a}\sum_{p \in p_a}(T - Z_a)(T - Z_a)^T$ (10)

$m_{bc} = \sum_{a=1}^{Cm}(Z_a - Z)(Z_a - Z)^T$ (11)

The d x $\bar{d}$ is the matrix A which is used for dimensionality reduction to make d dimensional features C = A^T x. The co- variance and mean matrix of all samples are given by,

$X = \frac{1}{n}\sum_{t \in t}(T - m)(t - m)^T$ (12)

Longitudinal disparity leads to increased class distinguishment. This is why the covariance function and its own vectors are so important. The assessed parameters are tested. This removes the smaller vector and the value is X. The similitude estimation and question data are calculated by comparing the score value (S_v). The compression gap from the image is investigated. The best fitness compression ratio is obtained .

$Compressed_{Fitness\ value}$=-40* q (-3*$\sqrt{\sum S_v}$)/2-exp($\sum \cos(3\pi * S_v)/d_b$)+10exp (13)

where q denotes the compressed wavelet and S_v is the compressed score value that is obtained. Finally the best rate of the compression can gets obtained.

Algorithm 1 (WICHO)

Input: Segmented image D_{n_fea}, Data_coordinate D_c

Output: Compressed image C_f

To compute compressed value,

For i=1:size($D_{n\_parameters}$,1)

For j=1:size($D_{n\_features}$, 1)

Distance(i,j)=$\sqrt{(i_{n_{features}}(i,1)}$-$i_{n_{features}}(j-1)$)+($i_{n_{features}}(i,1) - (i_{n_{features}}(j,1)^2$

End

End

data compressed features d_{n_fea}=[d_{n_fea}Distance]

To compute, score value d_{tv}= (d_{n_fea}dist)

Class label=unique(target)

K=length(class label)

For d=1:k

Temp=totalclassmean(I,:)

W(I,j)=-0.3* Temp* totalclassmean+log(i)

W(I,2:end)=temp

Wavelet data grouping

$\mathbf{Compressed_{Fitness\ value}}$**=-40* q (-3***$\sqrt{\sum S_v}$**)/2-exp(**$\sum \cos(3\pi * S_v)/d_b$**)+10exp**

End

d. cloud storage

The cloud services generally comprise online file storage, social networking and web mail. To protect the Cloud, the data or storage are secured. The technique of decryption is the opposite of encryption. Thus the preceding round values of both the data and the key provide the first round inputs for the decryption procedure. CTEA (Crack tetrolet elgamal algorithm) is a block cypher algorithm that transforms plain text in 64-bit blocks to cypher text using 48-bit keys. The number of rounds in CTEA is 16. Using a key-scheduling method, the 64-bit key is utilised to produce 16 keys, each of 48 bits, for each round. It's a symmetric key algorithm, which means it encrypts and decrypts data with the same key. The sequence may now be divided into equal bases. Then each split sequence may be decrypted in its own round. This can help to save both time and money. The ElGamal algorithm's security is predicated on the (supposed) difficulty of calculating discrete logs in a high prime modulus. When the data owner requests the file, the cloud server is in charge of creating a key and verifying it with the user for authentication.

For the purpose of key generation parameter can gets chosen.

1. Choose an integer K
2. Compute R=(G^kmod P)
3. Compute V=($K^{-1}(H(m) + X(r))$)
4. It is used for creating the per message or key

Once the signature can be verified after that we can ensure that the signature should be a valid one. Compute V and R both are equal means signature is valid

$$V=(g^{u^1} Y^{u^2} \text{Mod } P)\text{mod} q \quad (14)$$

$$R=(g^k \text{ Mod } P)\text{mod} q \quad (15)$$

$$R=V$$

Here the key generated can get distributed after that signing process can be done.

Hence to reduce the encryption, decryption time and cost here Split a pixel sequence into sub-sequences of equal bases and then decryption can be done . Here we can prove that the splitting of sequences can gradually reduce the decryption time and cost. Also the data lost cannot occurs in this process. Finally the decrypted file can be accessed by the user.

Algorithm 2 CTEA

```
Init(&ctx, key); CTEA
Printf("Plaintext message string is:%s\n, "plaintext string");
/ * Encrypt a plaintext message string * / *
printf("Crypted string is:);
If (len plaintext)
Left response = right call = 0UL;
/ * Break the message string for 64-bit (ok, 2 real-bit); + /-pad, if possible * / *
For (len block = 0; len block > < 4;
Left message = left answer < less than 8;
If (lens of complaint)
+ * string++ plaintext; len — plaintext;
}
left + = 0 other post;
}
(Strength block = 0; strength block < 4; strand
block + +)
Message row = message row less than 8;
Where (len plaintext).
Right message + = * string++ plaintext;
complaints: complaints —; complaints;
}
Right to message + = 0 else;
}
/ * Encrypt and screen files * / *
Enhanced Blowfish coding (& ctx, and left post, & right post);
printf('%lx%lx,' left message, right message);
/ * Under * / Update performance decryption
* ciphertext(navigation left)>24)=(uint8 t)(navigation left).
```

```
(controller+++ = (links to > > 16);
* ciphertext string+++(left message > > 8);
[108](1)capture on the left;
* strings++= ciphertext (uint8 t)(compare > > 24);
(string++) (uint8 t)(right>>16 message);
(uint 8 t)(message on the right > > 8));
(uint8t)communications right; (1)communications right;
+ = 8; len chip text
("\n"); \n
/ * Transform loop * / if decryption is necessary
}square("\n);
return 0;
}
```

5.RESULT AND DISCUSSION

Experiments for performance assessment are carried out in this section. In the MATLAB environment, the proposed scheme is implemented. Comparing the other existing approaches, the proposed scheme achieves a major increase with less workload and is also easily managed by a large consumer.

Table 1: Segmentation of the liver CT ROI and ROI areas along with compression

Data sets	Images	Input image	Ground truth image	Non-ROI (liver) compressed	ROI(cancer areas) compressed
Public Data Set (3DIRCADB)	Image 1		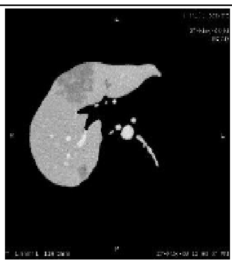	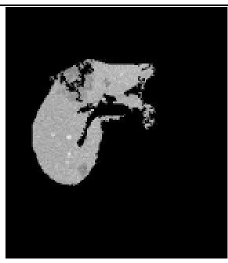	
	Image 2		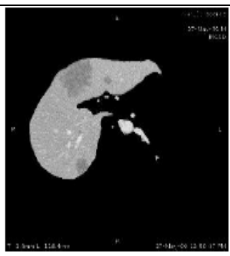	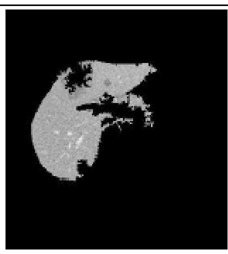	

	Image 3			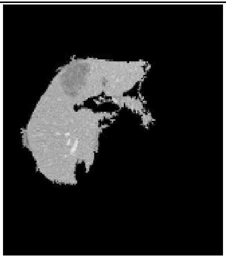	
	Image 4		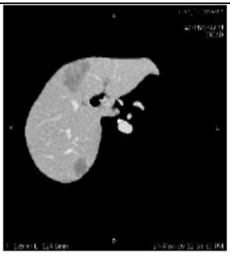	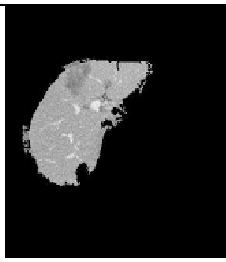	

Liver segmentation is achieved by using the Adaptive Contour in depth watershed segmentation method. 4 images from 27 sample pictures have been taken for the intent of testing. Table 1 displays segmented representations of the liver by means of a Adaptive Contour in depth watershed segmentation process, serves an accurate segmentation system for the separation of the ROI and Non-ROI.

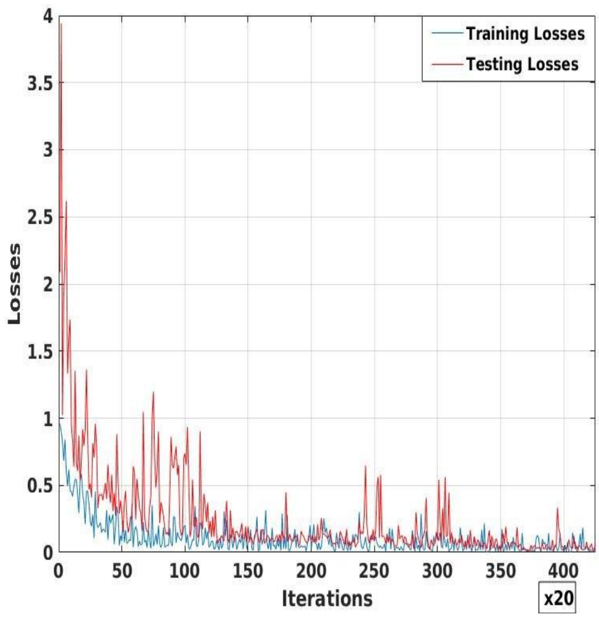

Figure 2 Iteration Vs. Losses

The training of the network was place over the course of 200 epochs using a single CPU at a learning rate of 0.001, and each epoch consisted of 760 iterations. Figure 2 presents the training process information that exhibit a loss vs the number of iterations. We found that the quality of the segmentation improved along with the amount of training images that were used.

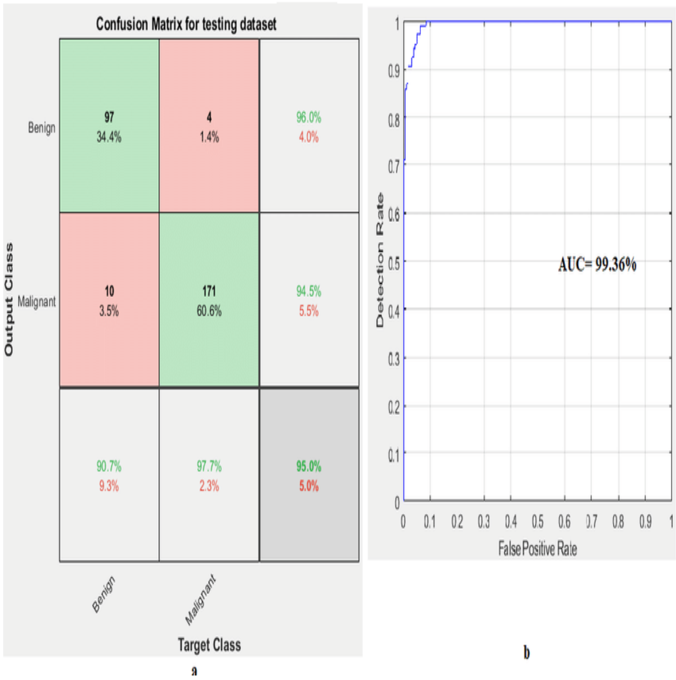

Figure 3 Calculation of AUC

Eighty percent of the dataset was designated for training, while the remaining twenty percent was used for testing and validation. The suggested system was evaluated using a confusion matrix in conjunction with an AUC (Area Under the Curve) calculated from a ROC (receiver operating characteristic) curve. The confusion matrix for the test data set is shown in Figure 3, along with the ROC that was calculated when the suggested system was applied to the dataset.

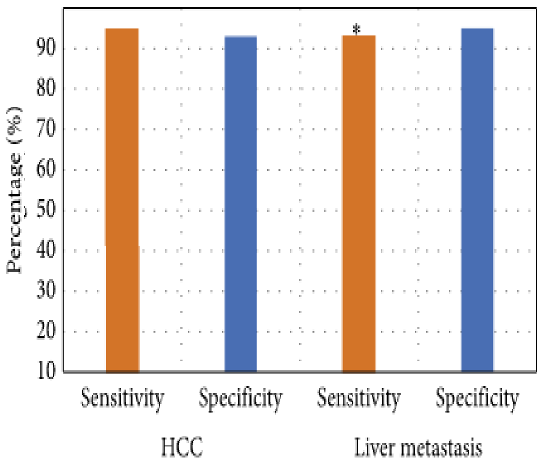

Figure 4 Stages of cancer predition

Figure 4 illustrates the percentage analysis of sensitivity and specificity of a CT examination to the liver tumor for instances of hepatocellular carcinoma (HCC) and liver metastasis. The algorithm suggested for segmentation can gets contrasted with [13],[14], [15], [20] to prove its efficiency.

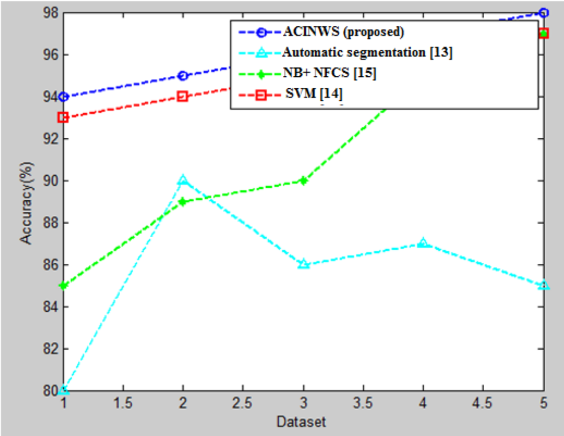

Figure 5 Determination of the accuracy percentile

The suggested ACINWS segmentation method exhibits a maximum 98 percent yield, which is superior than the existing approaches.

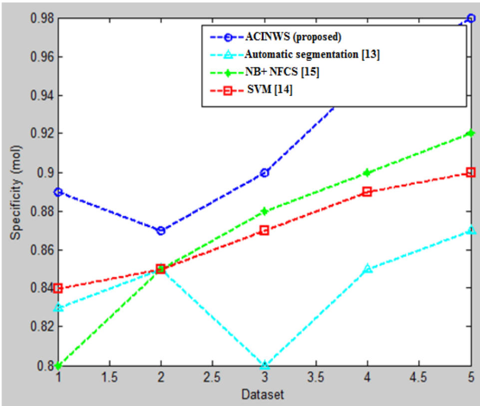

Figure 6 Data set vs. Specificity

In Figure 6, the quality of the specificity values that are arrived at using the existing approaches are compared by the suggested method. The findings show clearly that, compared to existing approaches, the suggested method achieved a greater specificities rate (98 percent).

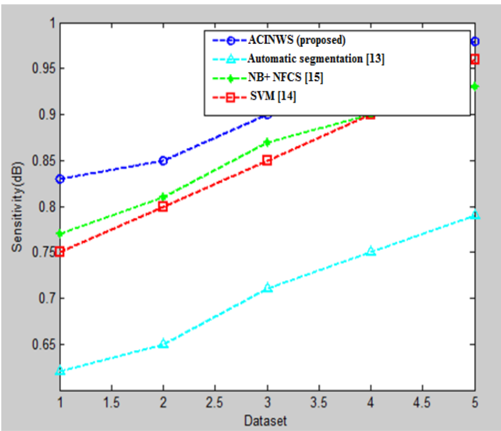

Figure 7 Data set vs. sensitivity

The figure in Figure 7 shows the approach presented which shows a greater sensitivity rate (98%) compared to the previous method. Then after segmentation the image can gets compressed and the compression parameters were discussed.

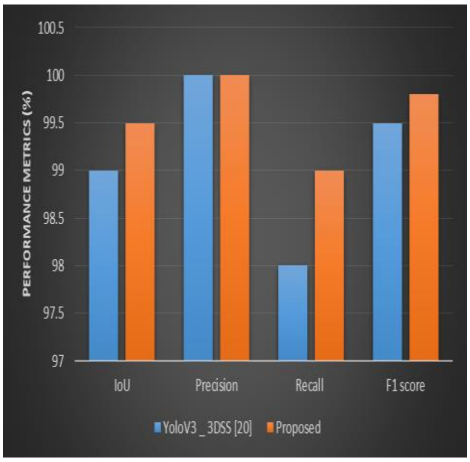

Figure 8 Performance metrics calculation

The results that were acquired from figure 8 indicated that the recommended approach had a higher range of IoU, accuracy, and F1score than the current mechanism that was being used at the time. In order to evaluate the efficacy of a segmentation technique, a binary mask derived from the segmented output is compared to the ground truth mask in order to determine the degree to which the two masks are similar. For the purpose of performance evaluation, a number of measures, including the dice similarity coefficient (DSC), accuracy, symmetric volume difference (SVD), and volumetric overlapping error (VOE), are taken into consideration.

Relative volume difference (RVD)

RVD refers to the proportion of change that may be seen when comparing the segmented picture to the ground truth. In this context, zero denotes a nearly perfect segmentation result. The equation that follows is the one that is used to determine accuracy.

RVD=|B|-|A|/|B| (16)

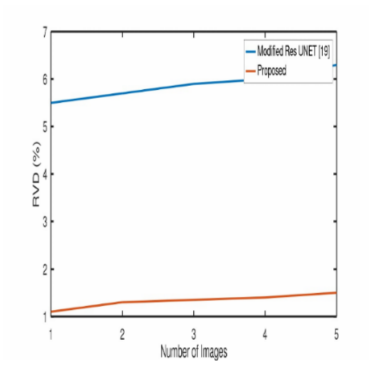

Figure 9 Number of images Vs. RVD

As can be seen from the picture, the suggested technique has an RVD that is noticeably lower than that of the other mechanisms that are already in existence.

Dice score

O and N represent the underlying data's attributes and those that were found, respectively. It is thus possible to calculate the Dice coefficient,

D(o,N)= (2o ∩ N/o+N) =2True Positive/2 True Positive +False Negative +False Positive (17)

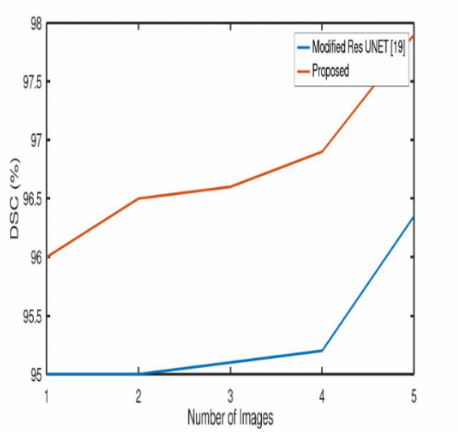

Figure 10 Number of images Vs. DSC

In the discipline of image processing, metrics such as the Dice score are used rather often for the purpose of assessing segmentation. When being trained for image classification tasks, instances of our proposed model are often tweaked for (weighted) cross-entropy. According to the results, the method known as ACINWS that was recommended is able to properly represent high values of the dice coefficients. This was shown to be the case by the researchers.

Volumetric overlapping error (VOE)

VOE stands for the volume overlap error that occurs between two different groups of voxels. Value of VOE lies between 0 & 1. A score of 0 shows complete segmentation in this case. The VOE may be calculated by using the following equation.

$$VOE = 1-\frac{2|A \cap B|}{|A|+|B|} \quad (18)$$

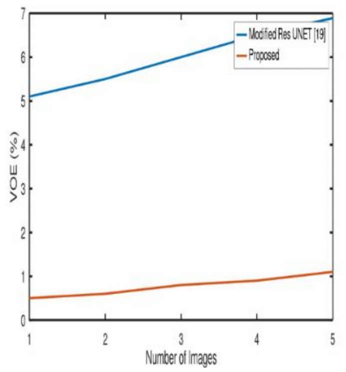

Figure 11 Number of images Vs. VOE

As of from the figure the proposed method have the very less VOE than that of the other existing mechanisms.

Table 2: Image Quality metrics

Parameters	Input image 1	Input image 2	Input image 3	Input image 4
PSNR	14.1913	13.2848	11.168	12.778
MSE	43.5359	54.1624	70.49	59.7
MD	222.1475	249.0821	249.05	232.1
PCR	100	100	100	100

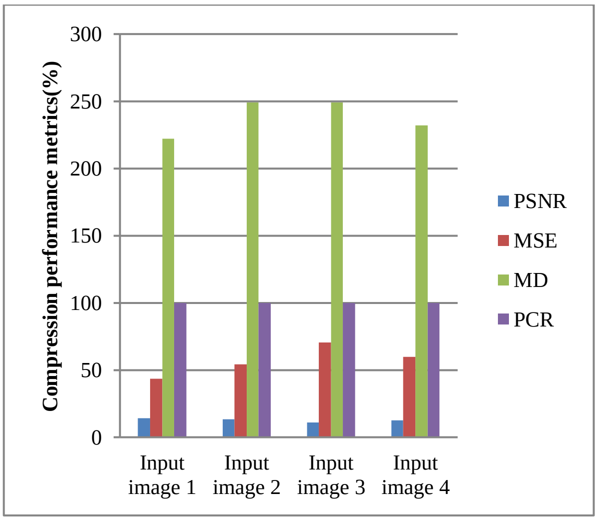

Figure 12 Image Quality metrics

The image reconstruction error (MSE), Signal to noise ratio (PSNR), Matching distance (MD), percent compression ratio (PCR) values are obtained as depicted in figure 12 . The satisfied results are obtained over the compression as depicted in table 2.

Table 3: Time and memory Analysis for Proposed CTEA technique

"File size"	" Key size"(bits)	"Encryption Time(ms)"	"Decryption Time(ms)"	"Memory(bits)"
5	**48.485**	**56473**	**41211**	**1121440**
10	**45.217**	**55876**	**40152**	**1211150**
15	**51.236**	**53147**	**39854**	**1284560**

20	**57.659**	**52471**	**38445**	**1322470**
25	**60.12**	**53450**	**39446**	**1322450**

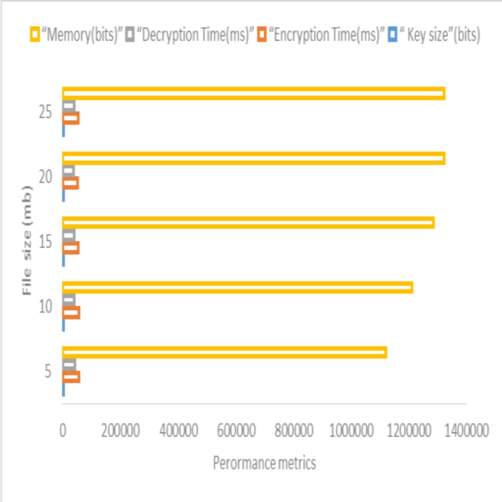

Figure 13 proposed method security analysis

The results of applying the suggested method to files of varying sizes are shown in Table 3 and Figure 13, respectively. When referring to the size of a file, megabytes are the unit of discussion (MB). The average key size is 48.489 bits, the encryption process takes 56471 milliseconds, and decrypting a 1 megabyte file takes 41211 milliseconds. To phrase it another way, there are 1121440 bits in a file that has a size of 1 megabyte when it is referring to memory. In addition, the duration of its execution, the timings of its encryption and decryption operations, as well as the amount of memory it allots, are detailed in Table 1.Then after the compression the encryption and decryption can be done by using the suggested CTEA algorithm and compared it can be compared with existing algorithms.Other current strategies such as DES **[16]**, RSA **[17]**, and AES **[18]** are compared to show the effectiveness of the proposed algorithm .

Table 4: Security analysis

	Security level (%)			
File size (mb)	**DES [16]**	**RSA [17]**	**AES [18]**	**Proposed**
20	78	77.23	73	80
40	80	85	76	85
60	83	88	80	90
80	85	80	79	95
100	90	90	85	93

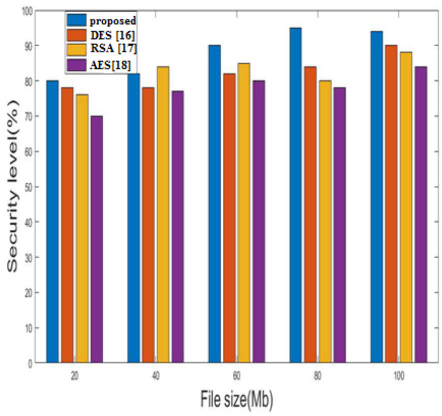

Figure 14 File size Vs. security level

Figure 14 and table 4 examines and compares the security levels of different encryption methods. DES, RSA, AES and the planned CTEA are the approaches explored. The security level in the file size of 20 MB is 80% LDHA, 78% DES, 77.23% RSA and 73% AES. Security levels for 40, 60, 80 and 100 MB of file size are also studied. The chart illustrates a high degree of security for the proposed CTEA compared to existing encryption approaches.

Table 5: Analysis of execution time

	Execution time (S)			
File size (mb)	**DES [16]**	**RSA [17]**	**AES [18]**	**Proposed**
20	5.8	4.6	4.8	3.5
40	3.8	4.2	4.2	3.8
60	3.2	3.2	3.5	2.9
80	4.2	4.2	3.3	4.2
100	3.3	4	4	3.9

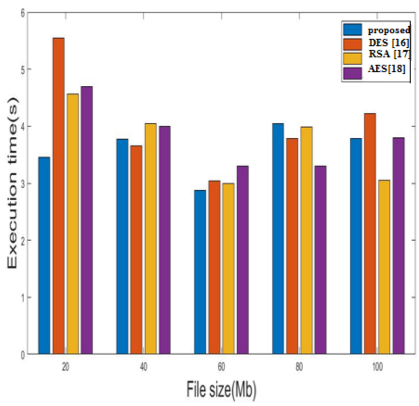

Figure 15 File size Vs. Execution time

Figure 15 and table 5 displays the efficiency of the proposed and current methods for various file sizes such as 20 MB, 40 MB, 60 MB, and 80 MB, as well as a comparison of execution times. The findings are evaluated and compared to other methods such as DES, RSA, and AES. As a consequence of the findings, it was discovered that the proposed approach outperforms than known methodologies in terms of performance. As of from the analysis it was revealed that the proposed mechanism has better performance ratios, especially at higher range of accuracy than other existing methodologies.

6.CONCLUSION

In this study, both the segmentation of liver tumors and the compression of images are covered. We segment livers and the tumours that it contains using a technique called the Adaptive Contour in depth watershed segmentation model. The modified watershed segmentation outperforms other architectures on the occasion of liver extraction and tumor segmentation with a very high DICE score, which is one of the primary contributions of the work. In this approach, the secure segmented image compression was done based on CTEA presented. Simulation outcomes illustrate that this process makes the greatest choice and identifies the best and the most appropriate route proficiently to compress the images, and in turn enhances the performance of compression by comparing other existing techniques. Thus, the proposed technique is better in offering better trusted compression system in the network system.

References

1. F. Brand, K. Fischer, and A. Kaup, "Rate-Distortion Optimized Learning-Based Image Compression Using an Adaptive Hierachical Autoencoder With Conditional Hyperprior," in Proceedings of the IEEE/CVF Conference on Computer Vision and Pattern Recognition, 2021, pp. 1885-1889.
2. F. Yang, L. Herranz, Y. Cheng, and M. G. Mozerov, "Slimmable compressive autoencoders for practical neural image compression," arXiv preprint arXiv:2103.15726, 2021.
3. V. Anusuya and V. S. Raghavan, "A Review on Medical Image Compression Using Wavelet Transform in Medical Images," Annals of the Romanian Society for Cell Biology, vol. 25, pp. 2925-2933, 2021.
4. C. T. Selvi, J. Amudha, and R. Sudhakar, "Medical image encryption and compression by adaptive sigma filterized synorr certificateless signcryptive Levenshtein entropy-coding-based deep neural learning," Multimedia Systems, pp. 1-16, 2021.
5. M. U. A. Ayoobkhan, E. Chikkannan, and K. Ramakrishnan, "Feed-forward neural network-based predictive image coding for medical image compression," Arabian Journal for Science and Engineering, vol. 43, pp. 4239-4247, 2018.
6. D. Yee, S. Soltaninejad, D. Hazarika, G. Mbuyi, R. Barnwal, and A. Basu, "Medical image compression based on region of interest using better portable graphics (BPG)," in 2017 IEEE international conference on systems, man, and cybernetics (SMC), 2017, pp. 216-221.
7. H. Sunil and S. G. Hiremath, "A combined scheme of pixel and block level splitting for medical image compression and reconstruction," Alexandria Engineering Journal, vol. 57, pp. 767-772, 2018.

8. S. A. Elhannachi, N. Benamrane, and T.-A. Abdelmalik, "Adaptive medical image compression based on lossy and lossless embedded zerotree methods," Journal of Information Processing Systems, vol. 13, pp. 40-56, 2017.
9. X. Song, Q. Huang, S. Chang, J. He, and H. Wang, "Lossless medical image compression using geometry-adaptive partitioning and least square-based prediction," Medical & biological engineering & computing, vol. 56, pp. 957-966, 2018.
10. Z. Liu, S. Li, Y.-k. Chen, T. Liu, Q. Liu, X. Xu, et al., "Orchestrating Medical Image Compression and Remote Segmentation Networks," in International Conference on Medical Image Computing and Computer-Assisted Intervention, 2020, pp. 406-416.
11. H. Amri, A. Khalfallah, M. Gargouri, N. Nebhani, J.-C. Lapayre, and M.-S. Bouhlel, "Medical image compression approach based on image resizing, digital watermarking and lossless compression," Journal of Signal Processing Systems, vol. 87, pp. 203-214, 2017.
12. Garg, D. K. . (2022). Understanding the Purpose of Object Detection, Models to Detect Objects, Application Use and Benefits. International Journal on Future Revolution in Computer Science &Amp; Communication Engineering, 8(2), 01–04. https://doi.org/10.17762/ijfrcsce.v8i2.2066
13. Pawan Kumar Tiwari, Mukesh Kumar Yadav, R. K. G. A. . (2022). Design Simulation and Review of Solar PV Power Forecasting Using Computing Techniques. International Journal on Recent Technologies in Mechanical and Electrical Engineering, 9(5), 18–27. https://doi.org/10.17762/ijrmee.v9i5.370
14. P. E. Sophia and J. Anitha, "Enhanced method of using contourlet transform for medical image compression," International Journal of Advanced Intelligence Paradigms, vol. 14, pp. 107-121, 2019.
15. M. Lavanya and P. M. Kannan, "Lung lesion detection in CT scan images using the fuzzy local information cluster means (FLICM) automatic segmentation algorithm and back propagation network classification," Asian Pacific journal of cancer prevention: APJCP, vol. 18, p. 3395, 2017.
16. V. N. Patil and D. R. Ingle, “A Novel Approach for ABO Blood Group Prediction using Fingerprint through Optimized Convolutional Neural Network”, Int J Intell Syst Appl Eng, vol. 10, no. 1, pp. 60–68, Mar. 2022.
17. F. Taher, N. Werghi, and H. Al-Ahmad, "Computer aided diagnosis system for early lung cancer detection," Algorithms, vol. 8, pp. 1088-1110, 2015.
18. R. Manickavasagam and S. Selvan, "Automatic detection and classification of lung nodules in CT image using optimized neuro fuzzy classifier with cuckoo search algorithm," Journal of medical systems, vol. 43, pp. 1-9, 2019.
19. R. Shivhare, R. Shrivastava, and C. Gupta, "An Enhanced Image Encryption Technique using DES Algorithm with Random Image overlapping and Random key Generation," in 2018 International Conference on Advanced Computation and Telecommunication (ICACAT), 2018, pp. 1-9.
20. Kadhim, R. R., and M. Y. Kamil. “Evaluation of Machine Learning Models for Breast Cancer Diagnosis Via Histogram of Oriented Gradients Method and Histopathology Images”. International Journal on Recent and Innovation Trends in Computing and Communication, vol. 10, no. 4, Apr. 2022, pp. 36-42, doi:10.17762/ijritcc.v10i4.5532.

21. V. Rao, N. Sandeep, A. R. Rao, and N. Niharika, "FPGA Implementation of Digital Data using RSA Algorithm," Journal of Innovation in Electronics and Communication Engineering, vol. 9, pp. 34-37, 2019.
22. X. Dong, D. A. Randolph, and S. K. Rajanna, "Enabling privacy preserving record linkage systems using asymmetric key cryptography," in AMIA Annual Symposium Proceedings, 2019, p. 380.
23. R. V. Manjunath, , & K.Kwadiki, "Automatic liver and tumour segmentation from CT images using Deep learning algorithm". Results in Control and Optimization, 6, 2022 100087.
24. Arellano-Zubiate, J. ., J. . Izquierdo-Calongos, A. . Delgado, and E. L. . Huamaní. “Vehicle Anti-Theft Back-Up System Using RFID Implant Technology”. International Journal on Recent and Innovation Trends in Computing and Communication, vol. 10, no. 5, May 2022, pp. 36-40, doi:10.17762/ijritcc.v10i5.5551.
25. J.Amin, , M. A.Anjum, M.Sharif, S.Kadry , A.Nadeem , & S. F. Ahmad . "Liver Tumor Localization Based on YOLOv3 and 3D-Semantic Segmentation Using Deep Neural Networks". Diagnostics, 12(4), 2022, 823.